

SEMI-ANALYTICAL ANALYSIS OF A RIGID ROTOR MOUNTED ON FOUR-PAD HYDROSTATIC SQUEEZE FILM DAMPER WITH SINGLE-ACTION MEMBRANE-TYPE RESTRICTORS

Ahmed KECHRA*, Ahmed BOUZIDANE*

*Research Laboratory of Industrial Technologies, Department of Mechanical Engineering,
Ibn Khaldun's University of Tiaret, BP 78 City, Tiaret, Algeria

ahmedkechra@yahoo.fr, ahmed.bouzidane@gmail.com

received 07 April 2023, revised 7 May 2023, accepted 10 May 2023

Abstract: The current study is a semi-analytical analysis of the vibratory behaviour of a rigid vertical rotor, supported by a new hydrostatic squeeze film damper (HSFD), consisting of four hydrostatic pads fed through four single-action membrane-type variable-flow restrictors. The Reynolds equation based on the Newtonian theory of lubrication is used and then adapted to our work, which is solved semi-analytically. In this paper, we study the effect of different parameters, the eccentricity, membrane geometry coefficient, pressure ratio and rotational speed, on the main characteristics of a four-pad HSFD. From the simulation results, we observed that at the critical speed, the rigid rotor fed by membrane restrictor shows a decrease in transmitted forces, a decrease in vibration response and good system stability as compared with a similar rotor fed by capillary restrictor. From the results reported in this work, we observed good agreement between our study and other works.

Key words: linear vibration, unbalance, hydrostatic squeeze film damper, Reynolds equation, Newtonian fluids, membrane restrictor, squeeze film lubrication

1. INTRODUCTION

The main and most common problem in the industry is the phenomenon of harmful vibrations resulting from imbalances in rotating machines, such as industrial turbo machinery, aircraft gas turbine engines and machining spindles. This has prompted many researchers to study the use of hydrostatic squeeze film dampers (HSFDs) as one of the effective solutions to control these vibrations. The latter has received increasing attention recently, due to its very low cost, durability and simplicity, with high efficiency in reducing the transmitted forces and increasing system stability.

Bouzidane et al. [1] investigated the effects of geometry, recess pressure and film thickness on the equivalent stiffness and damping of a four-pad hydrostatic journal bearing. In another work, Bouzidane et al. [2] studied the effect of rotational speed, supply pressure, pressure ratio, and viscosity on the transmitted force and unbalance response of a rigid rotor supported by a four-pad HSFD. In their work, a non-linear model was developed and the results obtained were compared with the simulation data of a linear model of HSFDs.

Many researchers have worked on the same topic. Abed et al. [3] analyzed three-pad HSFDs compensated with new electrorheological valve restrictors. Nemchi et al. [4] present a theoretical study of the effects of eccentricity ratio and Poiseuille Reynolds number on the performance of four-pad HSFDs. The results obtained indicate that the flow systems have a very significant impact on the performance of an HSFD loaded between pads. Benariba et al. [5] indicate that the micropolar effect is also mostly influenced by the stress ratio, on bearing performance. In another work [6], they deal with an analytical resolution of the modified Reynolds equation in order to study the effects of the coupling

number and the characteristic length of the micro-fluidic fluid on the transmitted forces, the vibratory response, the pressure profile and the flow.

Generally, there are two types of compensation: passive compensation, such as orifice and capillary restrictors, and active compensation [7–10]. In passively compensated bearings, the geometry of the compensating element never changes. However, in actively compensated bearings, the internal geometry is adjusted automatically by a pressure sensor.

In several works, contributions to the study of the behaviour of these externally pressed bearings with variable flow constraints have been made by Digast et al. [7], Mayer and Shaw [8], O'Donoghue and Rowe [9] and Cusano et al. [10]. The double diaphragm valve (membrane) was developed for grinding machine slide ways and spindle supports. It is a form of pressure sensing valve designed to control equal area opposed pad bearings. For high-performance practical purposes, this type of valve can be used to obtain infinite hardness as well as negative stiffness. The main advantage of the double diaphragm valve over the other systems is its manufacturing simplicity. Mohsin et al. [11] showed that the use of a membrane restrictor to compensate for the hydrostatic bearings enhances the static and dynamic stiffness of a bearing and reduces the power requirement. Morsi [12] discussed the performance of a hydrostatic thrust bearings compensated by passive and active restrictors from the point of view of fluid film stiffness and power requirement. Mohsin and Morsi [13] conducted both theoretical and experimental studies on the dynamic performance of a hydrostatic thrust pad bearing system compensated by variable resistance restrictors. Other important investigations which advocated the use of membrane restrictors as compensating elements in hydrostatic bearing systems to obtain better

performance characteristics are the studies of Degast [14] and Wang et al. [15], with diaphragm variable flow compensation, who studied the dynamic properties of externally pressurized, doubled pad, circular thrust bearings; they used Reynolds equation in cylindrical coordinates to simulate the pressure distribution and flow continuity. Sharma et al. and Singh et al. [16, 17] studied the influences of bearing flexibility and recess shape on the performance characteristics of multi-recess journal bearings, to determine the flow rate of membrane-type restrictor; they used the third-order polynomial of pressure difference.

Kang et al. [18, 19] used the coupled field to determine the flow rate between a rigid sill and elastic membrane. However, their simulation results do not provide a simple relationship between the flow rates or restriction coefficients and the pressure differences, which they used by using both analytical and experimental methods to study the membrane-type restrictor. Kang et al. [20, 21] used the identification method of restriction parameter, and deformation parameter for membrane-type restrictors obtained directly from the experimental results.

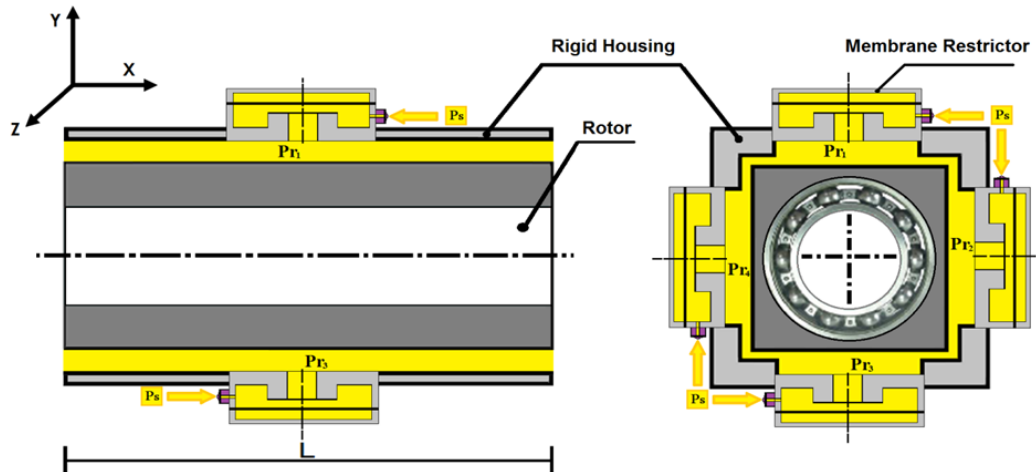


Fig.1. Schematic of a membrane-compensated four-pad hydrostatic squeeze film damper

As shown in Fig. 1, the fluid enters the membrane flow valve restrictor at a supply pressure (P_s), then escapes through the membrane clearance (x_0) and is then conducted through a line into a recess (P_{r0}). From the recess or pocket, the fluid escapes out of the bearing through the bearing clearances (P_a). If an external load (W) is applied, the pressure difference between the two opposite recess forces the membrane to move in such a way that the external resistance increases. If all the dimensions are properly chosen, the bearing may yield a much larger value of fluid film stiffness than that of fixed external restrictors. The membrane flow valve restrictor uses the gap height (x_0) as the variable. Because the flow resistance varies with the gap height, the diaphragm flow valve restrictor is a load sensing resistance that varies with the load; that is to say, the required change in resistance can be obtained through a precise diaphragm deflection.

In order to reach special results, we chose in the present work a semi-analytical analysis of the modified Reynolds equation to study the effects of pressure ratio, eccentricity, membrane geometry coefficient and rotational speed on the vibration response, transmitted forces and flow rate. For the selected operating conditions, quantitative changes in the performance characteristics of a four-pad, membrane-compensated HSFDF are compared with the previous results obtained for capillary compensation.

Certainly, the presented results obtained in this study are very useful for designers' tolerance.

2. PROBLEM FORMULATION

In this analysis, we adopt the assumptions given below:

- The bearing system is modelled as a two degree of freedom system.

- The pressure in the annular region is governed by the Reynolds equation, while that in the recess region it is assumed to be constant.
- The lubricant has a constant density and viscosity and is definitely incompressible.
- The flow is laminar in the membrane and in the bearing compensator.
- The relative ambient pressure is taken as zero.
- The inertia force of the lubricant is neglected.

3. FOUR-PAD HSFDF DESCRIPTION

Fig. 2(a) shows a rigid rotor supported by an HSFDF in the eccentric case composed of four identical plane pads fed through four single-action membrane restrictor-type hydraulic resistances. All pad geometries are equally spaced around the journal and are identical. The indices 1, 2, 3 and 4 refer to the characteristics of the lower, left and right hydrostatic flat pad, respectively. Each pad is fed by a membrane restrictor through a recess, which is supplied with an external pressure (P_s). Fig. 2(b) shows a longitudinal section of an HSFDF with four identical pads, and Fig. 2(c) shows the geometrical details of one of the four identical hydrostatic pads.

In our study, we will use the commonly used semi-analytical method. On one hand, it allows to reduce the size of the calculation programmes, while on the other hand, it requires the knowledge of the pressure in the cavity and the pressure at the free ends at each pad. The calculation of the characteristics of the HSFDF can be obtained through the juxtaposition of four hydrostatic flat pads.

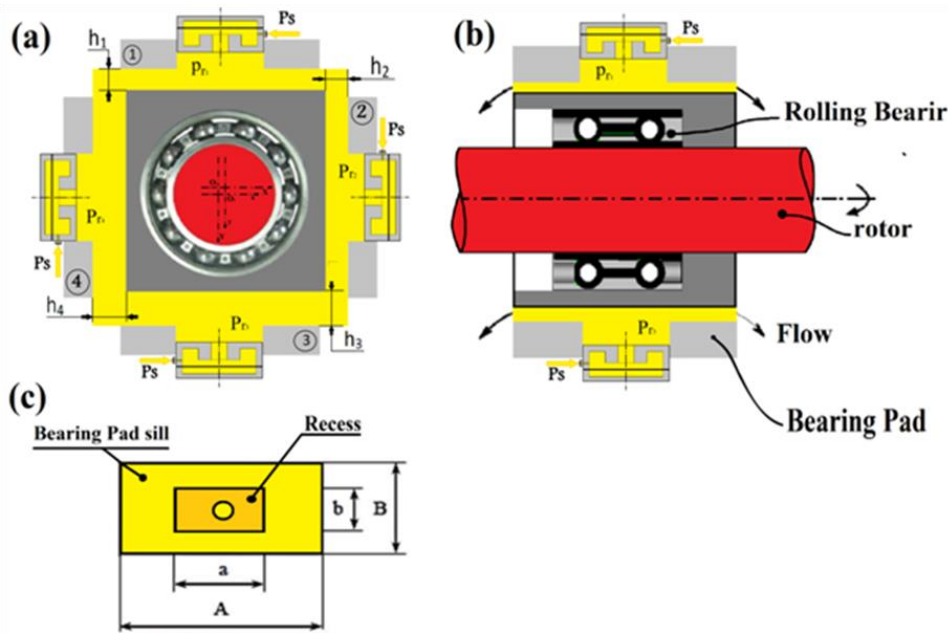


Fig. 2. (a) Four-pad HSFDF; (b) longitudinal section of a four-pad HSFDF; (c) geometric details of the hydrostatic pad

3.1 Reynolds equation

The Reynolds equation governs the pressure $P_i(x_i, z_i)$. In some cases, the equation can be solved semi-analytically by applying the infinitely short or long pad. If we assume that between the sheaths and the fluid there is no slip, the boundary conditions (Fig. 3.) associated with the field speed will be as follows:

- On pad ($y=0$) : $U_{1i} = 0$; $V_{1i} = 0$ et $W_{1i} = 0$
- On journal ($y=hi$) : $U_{2i} = 0$; $V_{2i} = h_i$ et $W_{2i} = 0$

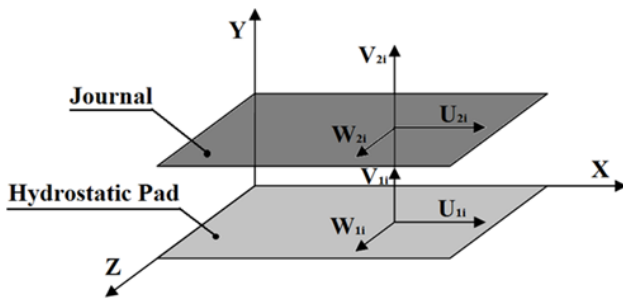


Fig. 3. Conditions for hydrostatic pad limits

The i^{th} hydrostatic pad: U_{2i} , V_{2i} and W_{2i} are the speeds surface of the runner and h_i is the squeeze velocity of the i^{th} hydrostatic pad ($i = 1, 2, 3$ and 4).

It is assumed that the recess is sufficiently deep to justify the assumption of the constant pressure. The housing of the rolling ball bearing is driven by a linear velocity (squeeze velocity) noted as V_{pi} .

We bind the centre of the Bearing of the fixed ence $(O_1, \vec{X}, \vec{Y}, \vec{Z})$, where O_1 : represents the centre of the bearing (Fig. 2a). The position and velocity of the housing relative to the centre are, respectively, defined in the Cartesian coordinates, where O_2 is the centre of the housing as:

$$\vec{O_1O_2} = x_1\vec{X} = y_1\vec{Y} \text{ and } \vec{V}(O_2) = V_a\vec{X} = V_b\vec{Y}$$

The geometric characteristics of four-pad HSFDFs are defined as follows:

- The number of pads n ($n = 4$)
- The size of the pad (Fig. 2c)
 - Outside dimension of the pad: A, B
 - The size of the races: a, b
- The dimension of the housing (Fig. 2b)

The knowledge of the film thickness and housing speed in each pad are given, respectively, in Fig. 2(a):

- Pad n°1: $h_1 = h_0 + x_1$
 $V_{p1} = \frac{\partial h_1}{\partial t} = V_a$ (1)
- Pad n°2: $h_2 = h_0$
 $V_{p2} = \frac{\partial h_2}{\partial t} = 0$ (2)
- Pad n°3: $h_3 = h_0 - x_1$
 $V_{p3} = \frac{\partial h_3}{\partial t} = -V_a$ (3)
- Pad n°4: $h_4 = h_0$
 $V_{p4} = \frac{\partial h_4}{\partial t} = 0$ (4)

Note that

$$\begin{cases} B' + h_1 + h_3 = Cte \Rightarrow h_1 + h_3 = Cte \\ A' + h_2 + h_4 = Cte \Rightarrow 2h_0 = h_2 + h_4 = Cte \end{cases} \quad (5)$$

where h_0 represents the film thickness with the housing in a centered position and x_1, V_a respectively, represent the linear displacement and squeezing velocity of the housing along the X -axis (Fig. 2a).

3.1.1 Calculations

In this study, we choose the semi-analytical method as it allows reduction in the programmes size. However, it requires knowledge of the pressure in the recess and the pressure at the free ends of each pad. Calculating the characteristics of four-pad HSFDFs therefore, it returns to calculate the characteristics of the four hydrostatic pads separately.

3.1.2 Infinitely long hydrostatic flat pad

The semi-analytical method is used to calculate the four-pad HSFDC characteristics, under the assumption of the infinitely long pad.

3.1.3 Calculation of pressure field

When A/B ratio (the length $A(A = L)$ to the width B) is big, the outflow in the Z direction is negligible compared with that in the X direction (Fig. 4b).

$$Q_{xi} \ll Q_{zi} \Rightarrow \frac{\partial P_i}{\partial x} = 0 \quad (6)$$

with

$$\begin{cases} Q_{xi} = Q_{xi}^+ + Q_{xi}^- \\ Q_{zi} = Q_{zi}^+ + Q_{zi}^- \end{cases} \quad (7)$$

where Q_{xi} is the flow rate along the X axis relative to the single-acting pad^{n°1} and Q_{zi} flow rate along the Z axis relative to the same pad.

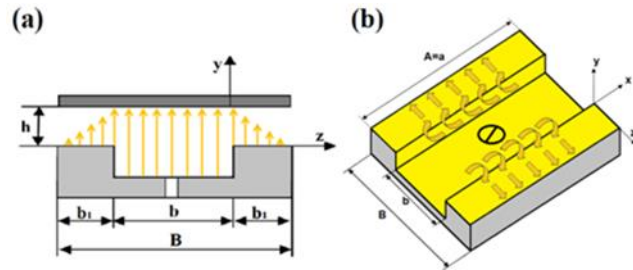


Fig. 4. Hydrostatic pad with infinite length. (a) Geometric details and longitudinal section and of hydrostatic pad with infinite length; (b) hydrostatic pad with infinite length

From Eq. (6), the pressure does not vary along the X axis, therefore the Reynolds equation for a single pad in direction $n^\circ 1$ is given as:

$$\frac{\partial}{\partial x} \left[\frac{h_i^3}{\mu} \left(\frac{\partial P_i}{\partial x} \right) \right] + \frac{\partial}{\partial z} \left[\frac{h_i^3}{\mu} \left(\frac{\partial P_i}{\partial z} \right) \right] = 12 V_{P_i} \quad (8)$$

which simplifies to:

$$\frac{\partial}{\partial z} \left(h_i^3 \frac{\partial P_i}{\partial z} \right) = 12 \mu h_i \quad (9a)$$

with

$$h_i = V_{P_i} = \frac{\partial h_i}{\partial t} \quad (9b)$$

The integration of Eq. (9) and the application of the boundary conditions in terms of pressure are:

$$P_i = P_{ai} \text{ for } Z = 0$$

$$P_i = 0 \text{ for } Z = b_1$$

The atmospheric pressure is taken as the reference pressure which allows us to have:

$$P_i = \frac{6 \mu h_i}{h_i^3} Z^2 - \left(\frac{P_{ai}}{b_1} + \frac{6 \mu h_i}{h_i^3} b_1 \right) Z + P_{ai} \quad (10)$$

This is valid for: $(b_1 + b) \leq Z \leq -b$

Particular case: for $\dot{h}_i = 0$ (static case)

$$P_i = P_{ai} \left(1 - \frac{Z}{b_1} \right) \quad (11)$$

$$0 \leq Z \leq b_1$$

$$P_i = \left(\frac{P_{ai}}{b_1} \right) (Z + b + b_1) \quad (12)$$

$$-(b + b_1) \leq Z \leq -b$$

3.2. Recess pressure

By resolving the following flow continuity equation, the recess pressure is determined for each hydrostatic pad as:

$$Q_{ri} = Q_{oi} \quad (13)$$

where

$$Q_{oi} = Q_{vi} + Q_{si} \quad (14)$$

Here Q_{vi} represents the squeeze flow of the i^{th} hydrostatic pad where:

$$Q_{vi} = S_i \dot{h}_i \quad (15)$$

Q_{ri} is the flow through the hydraulic resistance and Q_{si} the flow rate requirement of the i^{th} hydrostatic pad.

$$Q_{si} = Q_{sxi} + Q_{szi} \quad (16)$$

$$Q_{sxi} = \int_0^A dz \int_0^{h_i} u_{xi} dy \quad (17)$$

$$Q_{szi} = \int_0^B dx \int_0^{h_i} u_{zi} dy \quad (18)$$

$$u_{xi} = \frac{1}{2\mu} \frac{dP_i}{dz} y(y - h_i) \quad (19)$$

$$u_{zi} = \frac{1}{2\mu} \frac{dP_i}{dz} y(y - h_i) \quad (20)$$

where u_{xi} and u_{zi} are the flow velocities in directions x and z , respectively, of the i^{th} hydrostatic pads.

3.2.1. The total volumetric flow rate

The equation of the total volumetric flow rate is as follows:

$$Q_T = \sum_{i=1}^4 Q_{oi} = Q_{o1} + Q_{o2} + Q_{o3} + Q_{o4} \quad (21)$$

3.2.2. Flow equilibrium

3.2.2.1. Constant restriction of capillary

The equation of flow through the capillary to a recess can be determined as:

$$Q_{ci} = \frac{\pi d_c^4}{128 \mu l_c} (P_s - P_{ri}) \quad (22)$$

3.2.2.2 Single-action membrane-type variable restrictor

The external fluid is supplied by a hydraulic pump, which passes through the membrane restrictor and is fed into the recesses on the inner surface of the pad to form a fluid film, for

separating between the solid sliding surfaces in order to avoid contact of both solids.

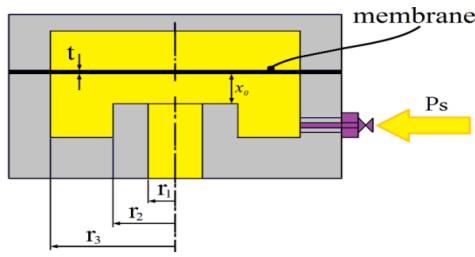


Fig. 5. Single action membrane-type restrictor [20]

In the membrane restrictor, as shown in of four-pad (Fig. 5), we find membrane thickness (t), Poisson's ratio (m), elastic modulus (E), membrane radius (r_3), radius of cylindrical sill (r_2) and radius of outlet from sill to recess (r_1); (x_0) is the initial opening when the membrane is subjected to only (P_s), and ($p_{ri} = 0$), and (x) is the equivalent opening as both pressures (P_s) and ($p_{ri} \neq 0$) act on the membrane. The flow rate through a single-acting membrane-type restrictor, to be obtained from the equation governing the viscous laminar flow between two parallel circular plates [20], can be determined by:

$$Q_{mi} = \frac{x_{mi}^3 \pi}{6\mu \ln(r_2/r_1)} (P_s - P_{ri}) = \frac{P_s - P_{ri}}{R_{mi}} \quad (23)$$

where (μ) is fluid viscosity, $x_{mi} = \delta + x_0$ is the gap between the sill and the membrane, (δ) is the membrane deflection, (x_0) is the initial gap after assembling and (R_{mi}) is defined as the flow resistance of this membrane-type restrictor as:

$$R_{mi} = 6\mu \ln(r_2/r_1) / \pi x_{mi}^3 \quad (24)$$

The membrane deflections vary with the radial position. In order to simplify the calculation of membrane deflection, the membrane deflections are assumed to be constant and equal to the membrane deflection at location (r_1), and so the membrane deflection can be expressed as:

$$\delta = K(P_s - P_{ri}) \quad (25)$$

where K is the deformation coefficient¹³ of the membrane:

$$K = 12(r_3^2 - r_1^2)^2 (1 - m^2) / 64Et^3 \quad (26)$$

3.3. Flow rate requirement

The total volumetric flow rate that must be supplied to the hydrostatic pad according to the x and y axes are given by the following equation:

$$\begin{cases} Q_{tx} = Q_{S2} + Q_{S4} \\ Q_{ty} = Q_{S1} + Q_{S3} \end{cases} \quad (27)$$

3.4. Carrying load capacity

The pad load for a length L relative to the pad $n^{\circ}1$ is:

$$W_{Pi} = \int_S P_i ds = \int_{S_1} P_{ai} ds + 2 \int_{S_2} P_i ds \quad (28)$$

where S are the contact surface, ds is an element of the surface, S_1 is the surface of the recess and S_2 is the surface pad sill.

After integration, we obtain:

$$W_{Pi} = P_{ai} L (b_1 + b) - \frac{2\mu h_i}{h_i^3} b^3 L \quad (29)$$

We can write this relationship in a more general form as:

$$W_{Pi} = P_{ai} S K_w - \frac{2\mu h_i}{h_i^3} b^3 L \quad (30)$$

where K_w is the coefficient of load, ranging from 0 to 1, as $K_w = 1 - (b_1/B)$. The relation (27) may also be written as:

$$W_{Pi} = \beta_i P_s S K_w - \frac{2\mu h_i}{h_i^3} b^3 L \quad (31)$$

where $\beta_i = P_{ai}/P_s$ is the ratio of the recess over the supply pressures.

The forces of the liquid film on the journal can be written as:

$$\begin{cases} W_x = W_{P2} - W_{P4} \\ W_y = W_{P1} - W_{P3} \end{cases} \quad (32)$$

where W_x and W_y are the load capacities in directions X and Y , respectively.

4. ROTOR DYNAMICS BEHAVIOUR

The rotor motion equation is given as:

$$\begin{cases} M\ddot{X} = (F_x + M\varepsilon_b \omega^2 h_0 \cos(\omega t)) \\ M\ddot{Y} = (F_y + M\varepsilon_b \omega^2 h_0 \sin(\omega t)) \end{cases} \quad (33)$$

The fluid film forces on the four-pad HSFD are

$$\begin{cases} F_x = F_{p3} - F_{p1} \\ F_y = F_{p4} - F_{p2} \end{cases} \quad (34)$$

where (e) is eccentricity, ($\varepsilon = e/h_0$) is eccentricity ratio and (h_0) is film thickness, (m) is mass of the rotor, ω is the excitation frequency, F_x and F_y are hydrostatic forces in the x and y directions, respectively, and F_{pi} ($i = 1, 2, 3$ and 4) is hydrostatic force of the i^{th} hydrostatic ad.

5. SOLUTION PROCEDURE

In order to study the non-linear dynamic behaviour of assembling a vertically rigid rotor, supported by HSFD fed by a membrane restrictor and using a Newtonian lubricant, we adopted the Newmark method, which is briefly discussed as follows.

Assuming that the assembly is rigid, the hydrostatic forces, which vary according to the change in velocity and eccentricity, are determined by applying the boundary and pressure field integral conditions, which is determined by solving Reynolds Eq. (8) in a semi-analytical method.

By solving the rotor motion Eq. (33) using non-linear methods, the flow rates, dimensionless vibration amplitude and transmitted force amplitudes are calculated.

The computed amplitudes are determined from direct numerical integration of the equations of motion by using a step-by-step method. For each frequency of excitation, the temporal responses are determined through the Newmark method.

The amplitude calculations for the first five periods yielded very adequate results. The negative pressure is set to zero during the interactive process of caring for the oil film cavities, and at each step the hydrostatic forces are determined. Film thickness and pressure are determined by solving the continuity of flow Eq. (13) of a given pressure ratio.

6. RESULTS AND DISCUSSION

6.1. Effects of pressure ratio

Fig. 6 shows the effects of the pressure ratio (β) and the speed of rotation on the dimensionless amplitude of vibration, the transmitted force and flow; for supply pressure 10 [bar], a viscosity of 0.0025 [Pa.s] and 0.2 of dynamic eccentricity unbalance.

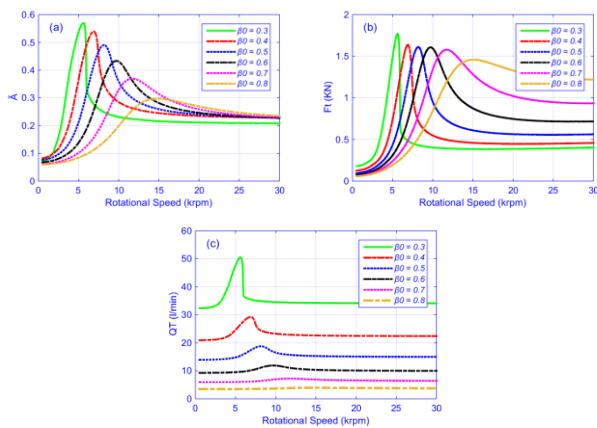


Fig. 6. Effects of pressure ratio on (a) variation of dimensionless vibratory amplitude, (b) variation of transmitted force amplitude and (c) variation of flow rate amplitude as a function of rotational speed

Panel (a) shows that, when the pressure ratio increases, the dimensionless vibration amplitude decreases due to the increase in film stiffness. We also record from panel (c) a decrease in the flow and in the transmitted forces (see (b)) as well.

6.2. Effects of the imbalance eccentricity

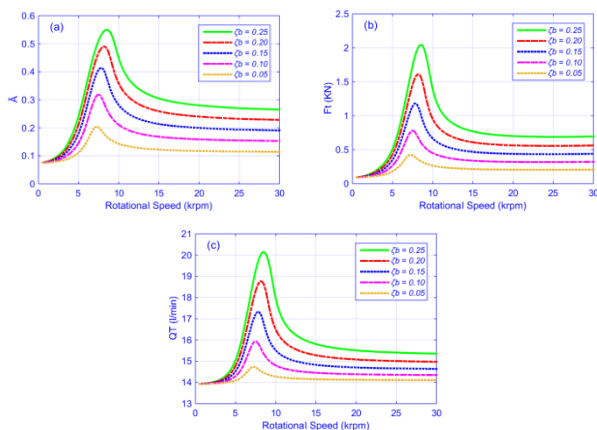


Fig. 7. Effects of imbalance eccentricity on (a) variation of dimensionless vibratory amplitude, (b) variation of transmitted force amplitude and (c) variation of flow rate amplitude as a function of rotational speed

Fig. 7 shows the effect of unbalance eccentricity (ζ_b) and the rotational speed on the dimensionless amplitude of vibration, the transmitted force and the flow rate for a supply pressure of 10 [bar], a pressure ratio $\beta = 0.5$ and a viscosity $\mu = 0.0025$ [Pa.s].

We can notice that in panel (a), when the eccentricity increases the vibration amplitudes also increase. The same can be noticed for transmitted force in panel (b), which can be explained by the increase in dynamic load. Panel (c) shows that the increase in flow is directly proportional to the speed of rotation and eccentricity.

6.3. Effects of membrane geometry coefficient

Fig. 8 shows the effect of the membrane geometry coefficient (a) and the rotational speed on the dimensionless amplitude of vibration, the transmitted force and the flow rate for a supply pressure of 10 [bar], a pressure ratio $\beta = 0.5$ with a viscosity $\mu = 0.0025$ [Pa.s] and $r_2 = ar_1, r_3 = ar_2$. It can be seen from panels (b) and (c) that the membrane geometry modulus is directly proportional to the flow rate and inversely proportional to the change in the transmitted force with very slightly reduced vibration amplitudes (a).

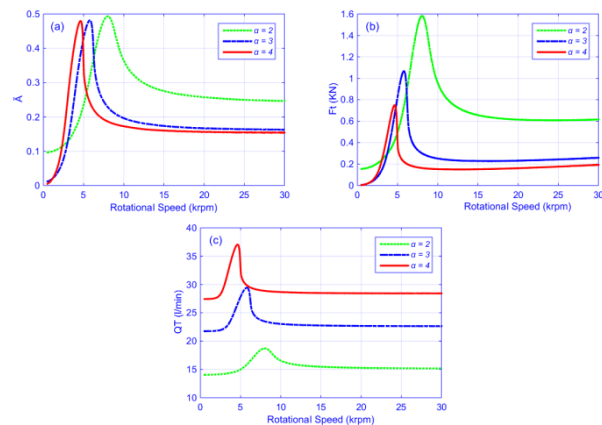


Fig. 8. Effects of membrane geometry coefficient on (a) variation of dimensionless vibratory amplitude, (b) variation of transmitted force amplitude and (c) variation of flow rate amplitude as a function of rotational speed

7. COMPARISON BETWEEN THE CAPILLARY MEMBRANE AND FLOW RESISTANCES

Let us represent, on the same graph, the analytical variance of dimensional vibration amplitude, transmission force and flow rate as a function of rotational speed, as shown in Fig. 9. It is clear from panels (a) and (b) that we obtained greater amplitude of vibrations and transmitted force thanks to the results presented in the curve obtained by the analytical code for capillary-type resistance as compared with the results of the semi-analytical code for a set with membrane-type resistance, and vice versa for flow (c). This leads us to state that the system supported by a membrane resistance is more stable.

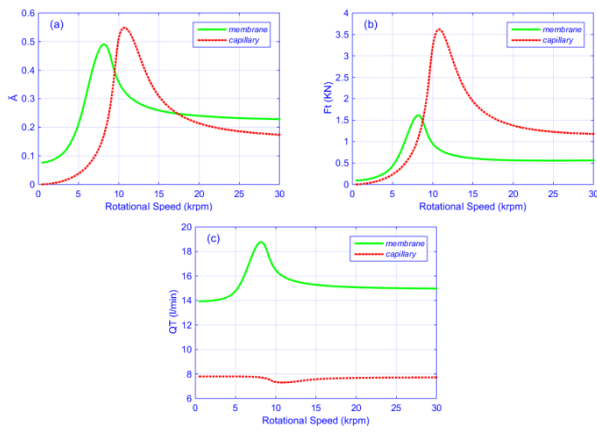


Fig. 9. (a) Dimensional vibration amplitude, (b) amplitude of the transmission force and (c) flow amplitude as a function of rotational speed for both capillary flow and membrane resistances

8. CONCLUSIONS

The aim of this research is to assess semi-analytically the performance of four-pad HSFDs with membrane-type variable flow restrictors as compensating elements.

The study focuses on the effects of the pressure ratio, membrane geometry coefficient, unbalance eccentricity and rotational speed on key parameters of the rotor dynamic behaviour. The role of HSFD is to control the vibration amplitudes, and to reduce the forces transmitted to the base, caused by the rotor imbalance. The conclusions can be summarized as follows:

- Effect of pressure ratio: due to the increase in compression ratio, we record a decrease in response amplitude, transmitted force and flow. When the rotational speed moves away from the critical speeds, changes in the compression ratio do not affect the amplitude of the response and stability is achieved.
- Effect of unbalance eccentricity: as expected, the amplitude of the response, transmitted forces and flux increase with increasing the unbalance eccentricity.
- Effect of membrane geometry coefficient: a lower membrane geometry modulus increases the transmitted forces with a lower flow rate, whatever the velocity. On the contrary, it leads to a very slight decrease in response amplitude when working near critical speed, due to increased damping.

From the analysis of the results and comparison of the two resistance properties of four-pad HSFD membranes and capillaries, we conclude that the membrane flow value is greater than capillary flow with a lower load and lower response amplitude, which allow good stability of the system.

Notation:


A	pad length	[m]
a	recess length	[m]
B	pad width	[m]
b	recess pad width	[m]
$F_X; F_Y$	represent the hydrostatic forces, in the X and Y directions	[N]
h_0	film thickness at the center position of the hydrostatic squeeze film damper	[m]
h_i	film thickness of the i^{th} hydrostatic pad	[m]
M	mass of the rotor	[Kg]
N	The speed of rotation	[tr/min]

O_1	Center of the bearing	[]
O_2	shaft center	[]
P_{ri}	recess pressure of the i^{th} hydrostatic pad	[Pa]
P_{r0}	recess pressure at the center position of the hydrostatic squeeze film damper	[Pa]
P_S	supply pressure	[Pa]
$Q_{xi}; Q_{zi}$	flow in the x , y and z direction respectively of the i^{th} hydrostatic pad	[m ³ /S]
Q_{Si}	lubricant outlet flow rate of the pad	[m ³ /S]
Q_{mi}	lubricant inlet flow rate of the membrane	[m ³ /S]
Q_T	total flow rate	[m ³ /S]
S_b	area of hydrostatic pad	[m ²]
S_r	area of hydrostatic recess	[m ²]
S	cross-section area	[m ²]
h_i	squeeze velocity of the i^{th} hydrostatic pad	[m/S]
$(u_{xi}; u_{zi})$	flow velocities in the x and y directions, respectively of the i^{th} hydrostatic pad	[m/S]
(x_i, z_i, y_i)	coordinate system used in the Reynolds equation	[m/S]
(x, y)	coordinate system used to describe the rotor motion	
β_0	ratio of recess pressure over supply pressure at the center position of hydrostatic squeeze film damper	[]
β_i	pressure ratio of the i^{th} hydrostatic pad	[]
ε	Unbalance eccentricity. (e_b/h_0)	[]
e_b	Eccentricity	[m]
μ	Viscosity	[Pa. s]
ω	excitation frequency	[rad/s]
E	elastic modulus	(N/mm)
x, x_0	gap and initial gap between sill and membrane	[m]
K_m	deformation coefficient of the membrane	(N/mm)
R_m	flow resistance of membrane restrictor	
r_1	exit radius	[m]
r_2	radius of restriction ring	[m]
r_3	Radius of the membrane	[m]
t	Thickness of the membrane	[m]
δ	membrane deflection	[m]
m	Poisson's ratio	[]

REFERENCES

1. Bouzidane A, Thomas M. Equivalent Stiffness and damping investigation of a hydrostatic journal bearing. Tribology transactions. 2007; 50 (2), 257-267. <https://doi.org/10.1080/10402000701309745>
2. Bouzidane A, Thomas M, Lakis A. Non linear dynamic behaviour of a rigid rotor supported by hydrostatic squeeze film dampers. Journal of tribology transactions of the ASME,2008; 130 (4), 041102-041102-9. <https://doi.org/10.1080/10402000701309745>
3. Abed A, Bouzidane A, Thomas M, Zhloul H. Performance characteristics of a three-pad hydrostatic squeeze film damper compensated with new electrorheological valve restrictors. Proc imeche, part j: j engineering tribology. 2017; 231, 889–899. <https://doi.org/10.1177/1350650116683622>
4. Nemchi A, Bouzidane A, Thomas M, Abed A. Performance analysis of four-pad hydrostatic squeeze film dampers loaded between pads under laminar and turbulent flow conditions. Tribol mater. 2018; surf inter, 12, 59-70. <https://doi.org/10.1080/17515831.2018.1441789>
5. Benariba A, Bouzidane A, Thomas M, Raynald G. Numerical analysis of a rigid rotor mounted on four-pad hydrostatic squeeze film damper lubricated with micropolar lubricant. Proc imeche, part j: journal of engineering tribology. 2018 ; 232, 513–524. <https://doi.org/10.1177/1350650117721119>

6. Benariba A, Bouzidane A, Thomas A. Analytical analysis of a rigid rotor mounted on three hydrostatic pads lubricated with micropolar fluids. *Proceedings of the institution of mechanical engineers, part j: journal of engineering tribology*. 2018; 0(0),1-11. <https://doi.org/10.1177/135065011880637>
7. Mayer JE, Shaw MC. Characteristics of externally pressurized bearing having variable external flow restrictors. *ASME journal of basic engineering*. 1963; 85, 291. <https://doi.org/10.1115/1.365657>
8. DeGast JGC. A new type of controlled restrictor (M.D.R.) for double film hydrostatic bearings and its application to high-precision machine tools. *Advances in machine tool design and research*, In: *Proceedings of the 7th international M.T.D.R. conference*, Birmingham. 1966 ; 12–16, 273–298. <https://doi.org/10.1115/1.2920582>
9. Rowe WB, O'donoghue JP. Diaphragm valves for controlling opposed pad hydrostatic bearings. *Engineer's Digest*. 1969; 30(4), 49.
10. Cusano C. Characteristics of externally pressurized journal bearing with membrane-type variable-flow restrictors as compensating elements. *Inst. of Mechanical Engineers, London*. 1974;188(52),527. https://doi.org/10.1243/PIME_PROC_1974_188_064_02
11. Mohsin ME. The use of controlled restrictors for compensating hydrostatic bearings. *Proceedings of the third international machine tool design research conference University of Birmingham*. 1963 ; 429–42.
12. Morsi SA. Passively and actively controlled externally pressurized oil-film bearings. *Trans ASME*. 1972; 56–63. <https://doi.org/10.1115/1.3451635>
13. Mohsin ME, Morsi SA. The dynamic stiffness of controlled hydrostatic bearings. *Trans ASME J Lub Tech*. 1969; 597–608. <https://doi.org/10.1115/1.3555006>
14. Degast JGC. A new type of controlled restrictor M.D.R for double film hydrostatic bearings and its application to high-precision machine tools. In: *Advances in machine tool design and research*, Oxford:Pergamon Press. 1966; 273–98.
15. Wang C, Cusano C. Dynamic characteristics of externally pressurized, double-pad, circular thrust bearings with membrane restrictors, *ASME J Trib*. 1991; 113,158–65. <https://doi.org/10.1115/1.2920582>
16. Sharma SC, Sinhasan R, Jain SC. Performance characteristics of multirecess hydrostatic hybrid flexible journal bearing with membrane type variable-flow restrictor as compensating elements. *Wear*. 1992; 152,279–300. [https://doi.org/10.1016/0043-1648\(92\)90126-S](https://doi.org/10.1016/0043-1648(92)90126-S)
17. Singh N, Sharma S C, Jain S C, Reddy S S. Performance of membrane compensated multirecess hydrostatic/hybrid flexible journal bearing system considering various recesses shapes. *Tribol Int*. 2004; 37, 11–24. [https://doi.org/10.1016/S0301-679X\(03\)00110-5](https://doi.org/10.1016/S0301-679X(03)00110-5)
18. Kang Y, Shen PC, Chang YP, Lee HH. Modified determination of fluid resistance for membrane-type restrictor. *Industrial Lubrication and Tribology*. 2007; 59(3),123-31. <https://doi.org/10.1108/00368790710746084>
19. Kang Y, Shen PC, Chang YP, Chiang CP. Modified predictions of restriction coefficient and flow resistance for membrane-type restrictors in hydrostatic bearing by using regression. *Tribology International*. 2007 ; 40(9),1369-80. <https://doi.org/10.1016/j.triboint.2007.03.002>
20. Kang Y, Chen CH, Lee HH, Hung YH, Hsiao ST. Design for static stiffness of hydrostatic bearings: single-action variable compensations. *Industrial Lubrication and Tribology*. 2011 ; 63 (2),103-18. <https://doi.org/10.1108/00368791111112225>
21. Kang Y, Chen CH, Chen YC, Chang C. Hsiao ST. Parameter identification for single-action membrane-type restrictors of hydrostatic bearings, *Industrial Lubrication and Tribology*. 2012;64(1),39-53. <https://doi.org/10.1108/00368791211196880>

Ahmed Kechra:  <https://orcid.org/0000-0002-1463-5600>

Ahmed Bouzidaine:  <https://orcid.org/0009-0001-9731-1870>



This work is licensed under the Creative Commons BY-NC-ND 4.0 license.